IEEE Access
The journal for rapid open access publishing

Received November 2, 2015, accepted November 27, 2015, date of publication December 4, 2015,
date of current version December 22, 2015.

Digital Object Identifier 10.1109/ACCESS.2015.2505726

Low Profile, Broadside Radiating, Electrically Small Huygens Source Antennas

RICHARD W. ZIOLKOWSKI, (Fellow, IEEE)
Department of Electrical and Computer Engineering, University of Arizona, Tucson, AZ 85721, USA
Global Big Data Technologies Centre, University of Technology Sydney, Sydney, NSW 2007, Australia

Corresponding author: R. W. Ziolkowski (ziolkowski@ece.arizona.edu)

This work was supported in part by the Australian-American Fulbright Commission and the Australian Defense Science and Technology Group.

ABSTRACT It is demonstrated numerically that a metamaterial-inspired, low profile (height approximately $\lambda/80$), electrically small ($ka = 0.45$) Huygens source antenna can be designed to radiate at 300 MHz in its broadside direction with a high radiation efficiency and a large front-to-back ratio. Two electrically small, near-field resonant parasitic (NFRP) antennas are first designed. Both are based on a coax-fed dipole antenna. An electric dipole response is obtained by combining it with a tunable Egyptian axe dipole (EAD) NFRP element. A magnetic dipole response is obtained by spatially loading the driven dipole with tunable, extruded capacitively loaded loop (CLL) NFRP elements. The driven dipole and the EAD and CLL NFRP elements are combined together and retuned to achieve a broadside radiating Huygens source antenna. Two different designs, one with two CLL elements and one with four, are obtained, and their performance characteristics are compared.

INDEX TERMS Directivity, electrically small antennas, Huygens source, metamaterial-inspired antennas.

I. INTRODUCTION

The desire for yet smaller mobile platforms continues to increase. This trend has generated an intense demand for printed electrically small antennas (ESAs) with superior performance characteristics. ESA improvements have become a significant technology enabler for wireless applications. Generally, omni-directional patterns are desired and they arise naturally from small, compact electric or magnetic dipole radiators [1]–[3]. The latter occur naturally as ESAs, i.e., when the size of the radiating structure is much smaller than the source wavelength. On the other hand, there are situations for which it is desirable to have higher directivity and/or to have a large front-to-back ratio (FTBR). In particular, it would be advantageous for a variety of applications to have the radiated power emitted primarily into one hemisphere. Examples include biomedical monitoring and on-body systems; point-to-point communications and wireless power transfer; mitigation of cell-phone specific absorption rate (SAR) issues; and radio frequency identification devices (RFIDs).

A variety of approaches to realizing higher directivity from small antenna systems have been considered. These include, for example, end-fire arrays [4]–[7], electromagnetic band-gap structures [8], high impedance surfaces and artificial magnetic conductors [9]–[12], Huygens sources [13], [14], near-field resonant parasitic (NFRP) elements [15], [16], and non-Foster circuit-augmented antennas [17].

While the printed, planar Huygens source antenna [13] has attractive performance characteristics, it nonetheless has a pattern that is maximum along a direction that lies in its plane and not orthogonal to it. It would be highly desirable to have an antenna that radiates orthogonal to its surface, like a patch antenna, but unlike the latter, be electrically small, require no ground plane, and still have a high FTBR. The desired radiated power behavior has been accomplished with NFRP elements [15], [16], but, unlike a patch antenna, are not low profile, i.e., they are around $\lambda/10$ in thickness, where λ is the free space wavelength corresponding to the operational frequency. Even the Huygens meta-surfaces [18]–[20] share this property due to a commensurate thickness of their unit cells. Similarly, the end-fire ESA arrays [4], [5] lose their attractive properties, in practice, when the distance between their elements is below $\lambda/10$. Can one design a simple unit cell that is about $\lambda/100$ in thickness and, hence, could be used to create an ultra-thin meta-surface, but could take advantage of the metamaterial-inspired antenna paradigm [21] and be used as a NFRP element to achieve an electrically small, low profile, broadside radiating element? Such an antenna design is reported for the first time in this paper.

All of the metal components in the reported antenna designs were taken to be copper with its known material parameters: $\varepsilon_r = 1.0$, $\mu_r = 0.999991$ and bulk conductivity $\sigma = 5.8 \times 10^7$S/m. All of the dielectric materials were taken to be the same as Rogers Duroid 5880 with material properties: $\varepsilon_r = 2.2$, $\mu_r = 1.0$ and loss tangent $tan\ \phi = 0.0009$. Several components are based on the Rogers Duroid 5880 copper cladded substrate that is 0.7874 mm (31 mils) thick with 0.5 oz copper, i.e., 0.017 mm thick copper. The operational frequencies of interest were arbitrarily selected to be near 300 MHz; the presented designs can be rescaled and tuned straightforwardly to other choices. The numerical simulations and their optimizations were carried out using the frequency domain ANSYS HFSS (high frequency structure simulator) ver. 14.0 [22].

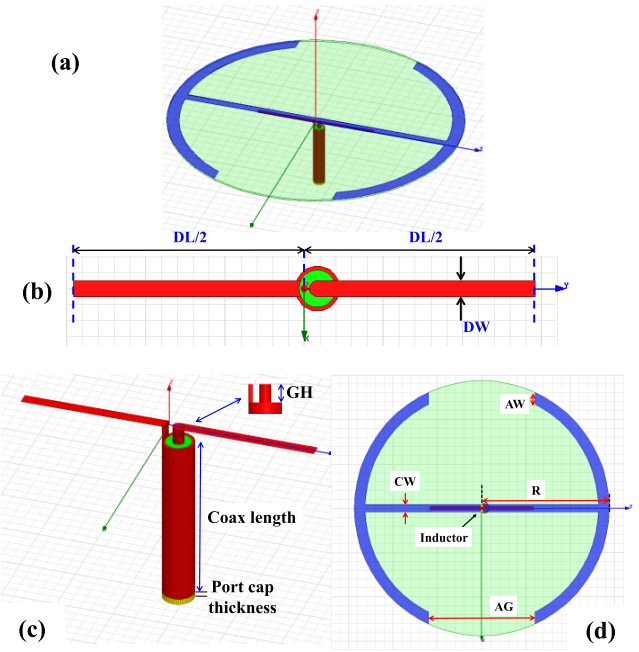

FIGURE 1. EAD NFRP antenna and its design parameters. (a) Isometric view, (b) top view of the coax-fed dipole, (c) isometric view of the coax-fed dipole, and (d) top view of the EAD NFRP element.

II. EAD NFRP ANTENNA

The first component of the design was the selection of the Egyptian axe dipole (EAD) antenna as the electric dipole radiator. This metamaterial-inspired NFRP antenna has become a standard component for many of our designs [21]. It is shown in Fig. 1. A printed dipole antenna is the driven element; it is fed with an air-filled coaxial cable. It lies on one side of a Rogers Duroid 5880 sheet. An EAD NFRP element with an inductor included in its middle is located on the other side of the sheet. The inductor allows for simple tuning of the resonance frequency [23], [24]. The common design parameters throughout this paper are (all physical dimensions will be given in millimeters): R = 72 (radius of both the EAD NFRP element and the dielectric disk), CW = 4, AW = 6, DW = 2, GH = 3, coax length = 30, inductor gap = 1.0, port cap thickness = 1.0, coax center conductor radius = 1.0, coax wall thickness = 0.5, and inner radius of coax outer wall = 2.238 (determined to produce a 50 Ω source through HFSS simulations of the coax with its copper outer wall). An HFSS waveguide port, 1W source is located at the end of the coax feed-line and, hence, the presence of the port cap is required. The input impedance is de-embedded to the top of the outer wall of the coax. The only parameters that will be varied to tune the EAD antenna and subsequent Huygens source antennas are the dipole length, DL; the EAD arc gap, AG; and the inductor value, L.

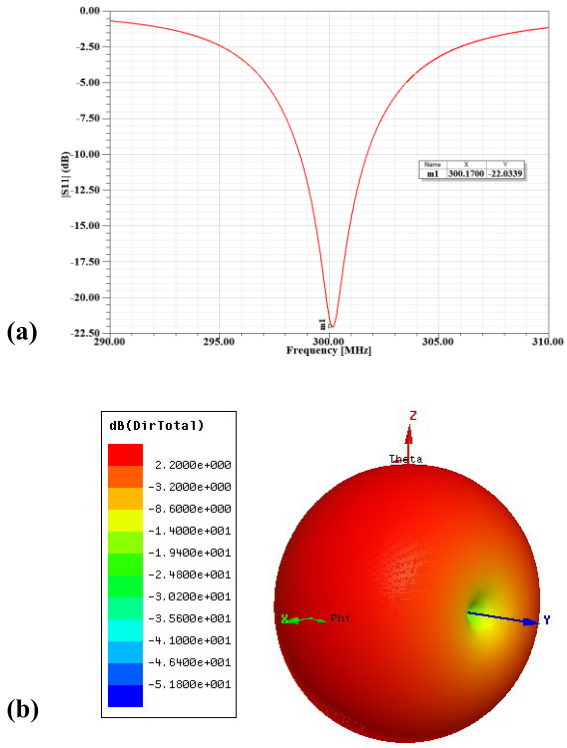

FIGURE 2. EAD NFRP antenna characteristics. (a) $|S_{11}|$ values as a function of the excitation frequency, and (b) 3D directivity pattern at f_{res} = 300.17 MHz.

The predicted performance characteristics of this EAD NFRP antenna with the remaining parameters set to: DL = 55, AG = 60, and L = 60 nH, are shown in Fig. 2. Fig. 2(a) demonstrates that the antenna is matched to the source at the resonance frequency $f_{res} = 300.17$ MHz with $|S_{11}|_{min} = -22.03$ dB. Thus, with a being the radius of the smallest enclosing sphere, $ka = 2\pi a/\lambda_{res} = 2\pi a f_{res}/c = 0.45$. The antenna is electrically small. Fig. 2(b) clearly demonstrates that it radiates as an electric dipole oriented along the axis of the EAD element (y-axis). The FTBR = 1.0 (0 dB). The accepted power AP = 0.994 W and the total radiated power RP = 0.962 W, giving the radiation efficiency RE = 96.8%. The maximum directivity $D_{max} = 1.64$ (2.15 dB). The peak realized gain $RG_{max} = 1.58$ (1.99 dB). The 3dB bandwidth is 9.52 MHz (giving a fractional bandwidth FBW = 3.17%).

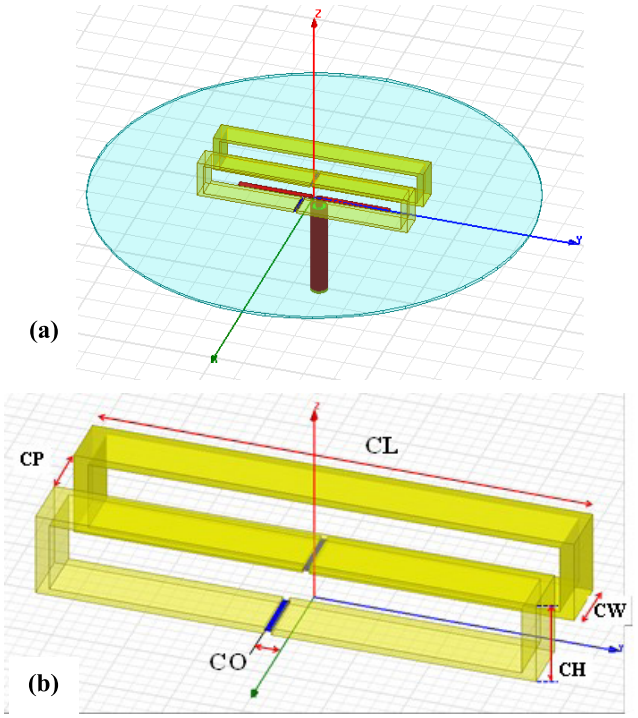

FIGURE 3. CLL-based NFRP antenna and its design parameters. (a) Isometric view of the entire antenna, and (b) isometric view of both CLL elements.

III. CLL-BASED NFRP ANTENNA

The second component of the Huygens source antenna design was the selection of CLL NFRP elements to be combined with the driven electric dipole antenna to create the magnetic dipole radiator. This low-profile antenna is shown in Fig. 3. The coax-fed dipole is again on the bottom side of the Duroid sheet. Two copper, extruded CLL elements lie flat on the top of the sheet and are parallel to the dipole axis and equally spaced from it, the y-axis. Each is loaded with a capacitor with capacitance C across an offset 1.0 mm gap. These capacitors allow tuning of the CLL resonances.

The copper CLL elements are simply extruded rectangular versions of the printed protractor antenna NFRP elements [25]. Consequently, the radiation physics is the same. The dipole is electrically coupled to the CLLs through its electric field, which excites currents along the long direction of the CLLs. With the offset capacitor, loop modes are generated and the magnetic dipole behavior occurs. Because the electric field is symmetric on both sides of the dipole axis, both CLLs generate the same loop mode and, hence, their magnetic dipoles reinforce each other. This physical behavior is comparable to that realized by the two protractor NFRP elements in the planar Huygens source antenna [13].

In all cases, the dimensions were: the CLL total length, CL = 70; the CLL width, CW = 8; the distance between the CLLs, CP = 8; and the total CLL height, CH = 12. The capacitor offset distance, CO = −2.5, along the y-axis from the origin to the center of the gap. The value of the capacitance C and the dipole length DL were the only parameters adjusted to fine tune this CLL-based antenna and the subsequent Huygens source antennas. The horizontal strips of the CLL elements are 1.0 mm thick (hence, the distance along the z-axis between the top of the bottom strip and the bottom of the top strip is 10 mm) while their vertical end-strips are 2.0 mm thick (along the y-axis). The thicker copper at the ends was found to provide an easier path for the loop currents to form. The thicker copper and extruded CLL versions improved the radiation efficiency significantly in comparison to initially tested Duroid-based CLLs. The emphasis on high efficiency is dictated by the very efficient EAD NFRP antenna and the need for equal amplitude fields radiated from both the electric and magnetic dipoles to achieve the Huygens source. Including the dielectric thickness, the Duroid copper thickness and the CLL height, the total height of this antenna is 12.8044 mm. While the overall antenna size could have been made smaller by varying the length, width, and height of the CLL elements and the capacitance C to achieve the same resonance frequency, the Duroid disk size was maintained since it will be the same size for the EAD NFRP element in the Huygens source design.

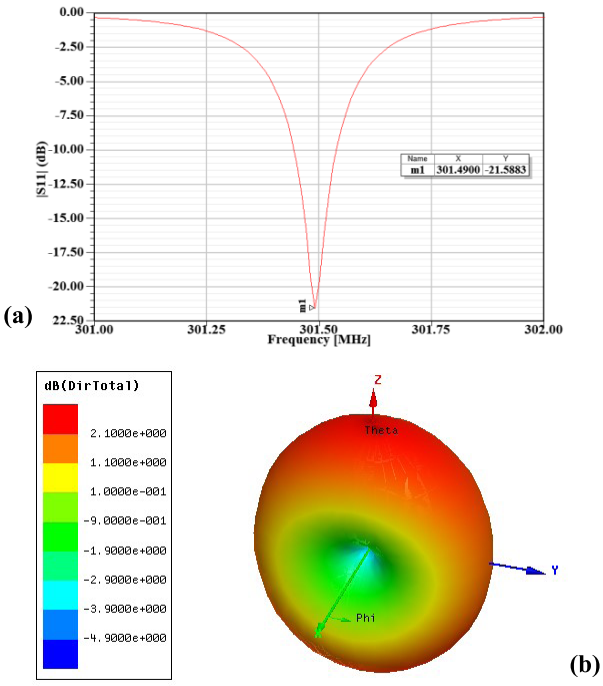

FIGURE 4. EAD NFRP antenna characteristics. (a) $|S_{11}|$ values as a function of the excitation frequency, and (b) 3D directivity pattern at f_{res} = 301.49 MHz.

With DL = 50 and C = 5.0 pF, the predicted performance characteristics of this CLL-based NFRP antenna are shown in Fig. 4. Fig. 4(a) demonstrates that the antenna is matched to the source at the resonance frequency f_{res} = 301.49 MHz with $|S_{11}|_{min}$ = −21.59 dB. Thus, ka = 0.45 and this antenna is also electrically small. The height of the antenna at its resonance frequency is approximately $\lambda_{res}/78$, confirming that it is very low profile. Fig. 4(b) clearly demonstrates that

it radiates as a magnetic dipole oriented along the x-axis and perpendicular to the axis of the electric dipole radiator (y-axis). The FTBR = 1.0 (0 dB). The accepted power AP = 0.993 W and the total radiated power RP = 0.884 W, giving the radiation efficiency RE = 88.4%. The maximum directivity D_{max} = 1.61 (2.07 dB). The peak realized gain RG_{max} = 1.42 (1.52 dB). The 3dB bandwidth is only 0.29 MHz (FBW = 0.096%). While having very good radiation efficiency, this bandwidth is quite narrow. It was expected that the magnetic dipole bandwidth would be smaller by at least a factor of 2 according to the fundamental bounds on the quality factor Q [26] and previous experiences with NFRP antennas [21]. The very small bandwidth occurs because the actual radiating elements are the CLLs and their radius is smaller by more than half of the EAD radius and they fill only a very small portion of the Wheeler sphere. While this was initially expected to be a "show stopper" in achieving the Huygens source antenna, it thankfully was not.

IV. 2 CLLs - 1 EAD HUYGENS SOURCE ANTENNA

The Huygens source antenna was obtained by merging together the EAD and CLL NFRP designs. The first major difficulty was remembering that to achieve a Huygens source, the phase centers of the electric and magnetic dipoles must be very close to one another. The original EAD NFRP element rested on top of the Duroid sheet. All attempts to simply leave the EAD on this plane in the presence of the CLLs did not work. Either the electric or magnetic dipole behaviors would remain separately or dominate depending on the parameters.

The phase center of the magnetic dipole which is generated by a CLL NFRP element lies near its geometrical center. This seemingly small distance – about 6 mm with nearly a 1000 mm wavelength – significantly impacted the process of tuning the electric and magnetic dipole behaviors to overlap. Once it was recognized as being the dominant factor, the design proceeded numerically with straightforward parameter optimization. The resonance frequencies of both the electric and magnetic resonators simply had to be close to each other initially.

However, to move the EAD NFRP element vertically, a choice had to be made. Should the dielectric be left with the driven dipole or kept with the EAD element? On the other hand, since they rest on it, the dielectric with the dipole source is necessary for the CLL-based radiators. To avoid redesigning everything, it was decided that the dielectric should be kept with both the dipole source and the EAD element. Thus, the integrated design proceeded with having two Duroid sheets, one for the driven dipole and one for the EAD element. It actually would simplify the fabrication of this antenna. This final configuration is shown in Fig. 5. The offset distance, OZ, is measured along the z-axis from the origin to the bottom surface of the EAD's Duroid sheet, the EAD element being on its top surface. While no material was used in the model to support the EAD element, a Rohacell or Styrofoam disk would provide effectively the same properties at the frequencies of interest.

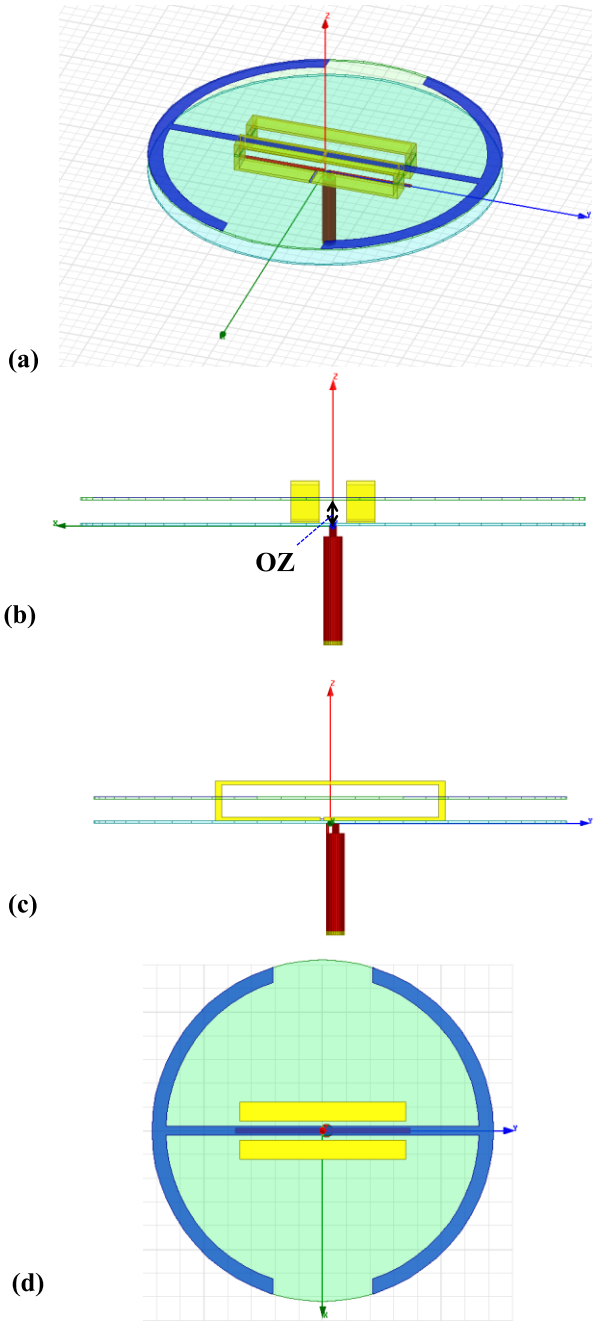

FIGURE 5. Huygens source antenna with one EAD and two CLL elements. (a) Isometric view, (b) end view, (c) side view, and (d) top view.

With the length tuning parameters set at: DL = 73.5, AG = 42, and OZ = 7.28; and the lumped element parameters set at: L = 56 nH and C = 5 pF, the HFSS predicted performance characteristics of this Huygens source antenna are shown in Fig. 6. Fig. 6(a) demonstrates that the antenna is well-matched to the source at the resonance frequency f_{res} = 299.17 MHz with $|S_{11}|_{min} = -26.35$ dB. Thus, ka = 0.45. The antenna is electrically small and very low profile ($\sim\lambda_{res}/78$). Figs. 6(b) and 6(c) clearly demonstrate that it radiates as a Huygens source broadside

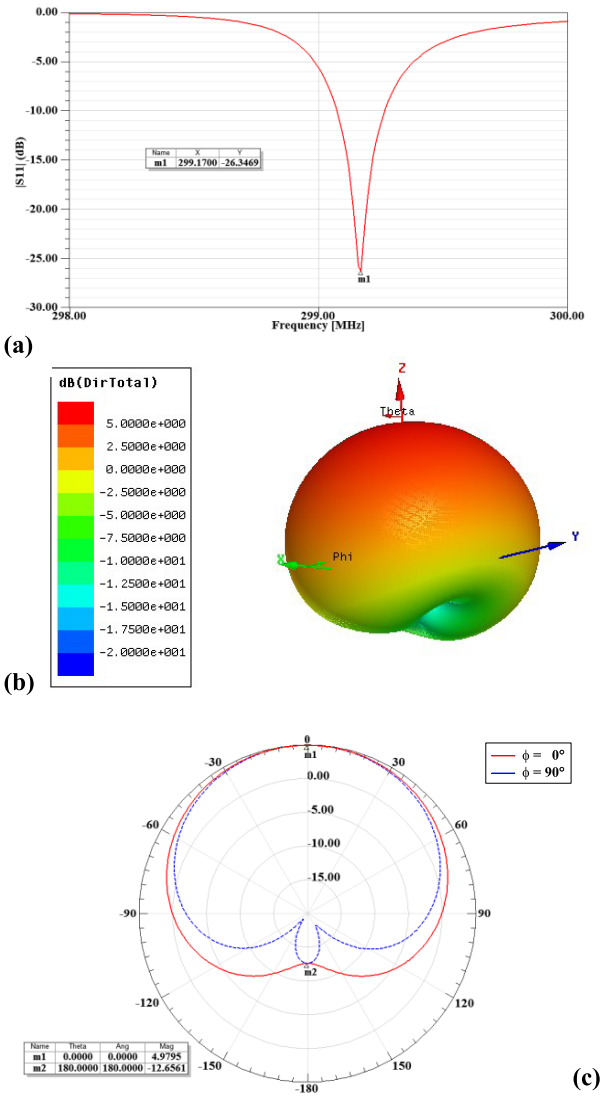

FIGURE 6. HFSS-predicted performance of the Huygens source antenna with two CLL and one EAD NFRP elements. (a) $|S_{11}|$ values versus the excitation frequency, and (b) 3D directivity pattern, and (c) 2D directivity patterns at $f_{res} = 299.17$ MHz.

to the plane of the antenna, i.e., along the z-axis. The FTBR = 58.04 (17.64 dB). The accepted power AP = 0.998 W and the total radiated power RP = 0.877 W, giving the radiation efficiency RE = 87.9%. The maximum directivity D_{max} = 3.15 (4.98 dB). The peak realized gain RG_{max} = 2.76 (4.41 dB). The 3dB bandwidth is 0.59 MHz (giving a fractional bandwidth FBW = 0.20%).

The physics associated with this antenna is interesting because the net design involves two strongly coupled resonators, one electric and one magnetic. The EAD and CLL elements are themselves associated, respectively, with capacitive and inductive effects. However, when they are in the presence of each other's intense near fields, the coupling effects play a major role. As already noted, the alignment of the CLL NFRP elements with respect to the electric field of the driven dipole stimulates their response. In the presence of the EAD NFRP element, which is also driven by that electric field, strong capacitive coupling between them occurs. Being electric-oriented by its nature, this additional capacitance actually impacts the EAD behavior more. This is clearly recognized by the change in the design parameters needed to achieve the optimized Huygens design. There were no changes made to the CLL elements. On the other hand, the smaller inductance value, L, increases the 50 Ω frequency point associated with the input resistance curve. This compensates for the increased capacitance associated with the coupling, which decreases that frequency point. However, because L was restricted in this case by choice to be an integer, some fine tuning was needed and was provided by the small capacitance increase associated with the decrease in the gap size AG. While the input resistance was nearly right, the overall system had too much capacitive reactance for matching to occur. This mismatch was then corrected by the significant increase in the length of the driven dipole, which provided the needed inductance shift of the input reactance curve. These effects are further emphasized below with the 4 CLL element design.

As noted, the optimized OZ value places the EAD at 5.4756 mm from the inside face of the bottom legs of the CLL elements, just 0.4756 mm above their physical centers. This choice, which was determined through a series of simulations varying OZ, provided the necessary alignment of the phase centers associated with the two resonators. There were minor tradeoffs between the peak FTBR value and the degree of matching that resulted from the choice of precision in each design parameter.

The fact that the two NFRP elements are strongly coupled resonators is further emphasized by the significant phase change in the currents along the EAD that results when OZ is too large. When OZ is small, the EAD is more strongly coupled to the driven element and its behavior is dominant. When OZ becomes larger, the relative strengths of the electric and magnetic dipoles become closer. When OZ is a bit too large, the CLL behavior is dominant. However, when OZ is very large, the EAD actually becomes driven by the currents on the top long segment of the CLL elements, which flips the direction of its radiated electric field. The combined system then radiates along the negative z-axis.

This outcome is demonstrated in Fig. 7. With OZ = 7.5 mm, Fig. 7(a) indicates that the antenna remains well-matched to the source at the nearby frequency of 299.31 MHz, a slight 0.14 MHz blue-shift. However, Fig. 7(b) shows that the maximum of the power radiated by the Huygens source is now directed along the negative z-axis. This π phase transition occurs from a change in sign of the current direction on the EAD element.

Finally, it is noted that the larger bandwidth of the EAD element and the narrower bandwidth of the CLL elements produced an antenna whose bandwidth is in between the two. Because each NFRP element is highly resonant, one would have expected a narrow bandwidth with any final design.

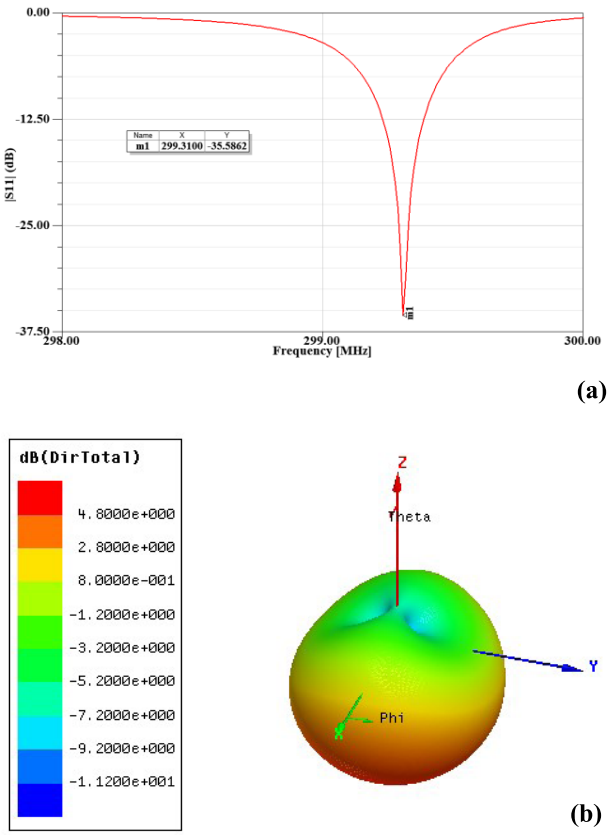

FIGURE 7. Illustration of the phase transition that occurs when the distance OZ is increased too much. (a) $|S_{11}|$ values as a function of the excitation frequency, and (b) 3D directivity pattern at f_{res} = 299.31 MHz, when OZ = 7.5 mm.

What is remarkable is that the very narrow bandwidth of the CLL elements did not prevent the Huygens source from happening. As long as there was significant overlap of the CLL-based and EAD-based antennas' $|S_{11}|$ curves, i.e., the resonance frequencies of the integrated electric and magnetic resonators were near each other, the desired Huygens source effect could be obtained and the associated bandwidth of the optimized design fell between the values of the component structures.

V. 4 CLLs - 1 EAD HUYGENS SOURCE ANTENNA

To further explore the physics of the design, two more CLL elements were added to it. This choice was made to learn if more magnetic dipole contributors were included, would the overall efficiency, FTBR and bandwidth values change. The only additional design parameter was the location of these added elements. While it was noted that CP = 8 mm, this meant that each of the two CLL elements was 4 mm from the dipole axis. Consequently, the two additional CLL elements were simply placed 4 mm from the other two, further away from the dipole axis. This design is illustrated in Fig. 8(a).

With the length tuning parameters set at: DL = 75, AG = 42, and OZ = 7.55; and the lumped element

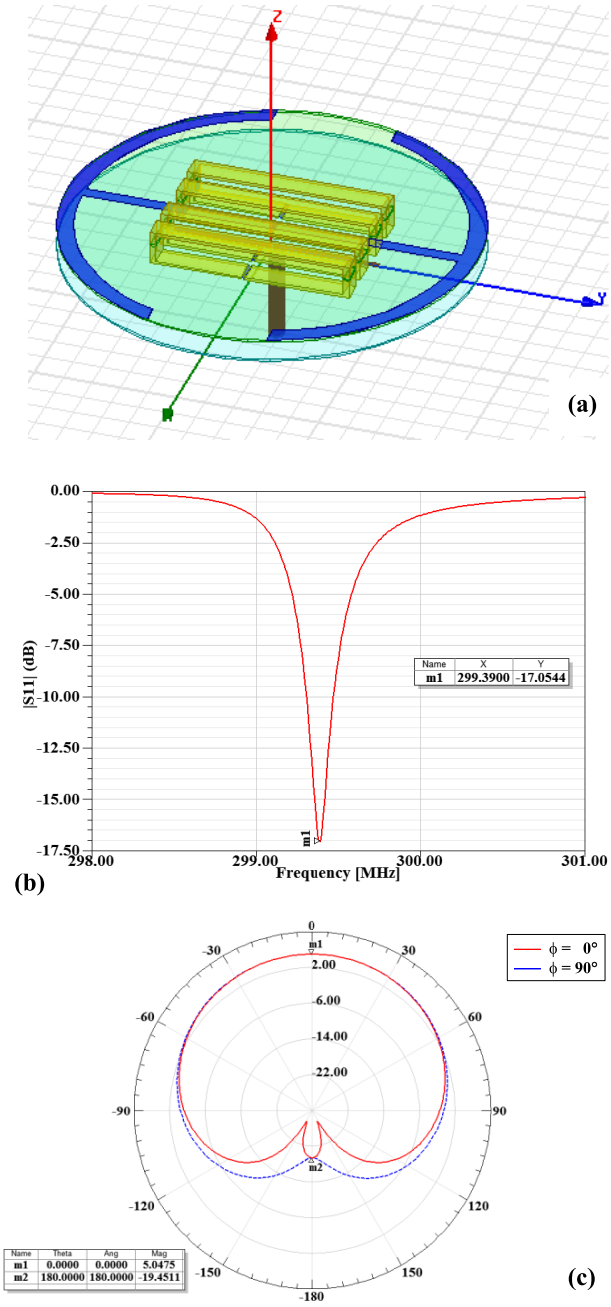

FIGURE 8. HFSS-predicted performance of the Huygens source antenna with four CLL and one EAD NFRP elements. (a) Isometric view, (b) $|S_{11}|$ values versus the excitation frequency, and (c) 2D directivity patterns at f_{res} = 299.39 MHz.

parameters set at: L = 56 nH and C = 4.2 pF, the HFSS predicted performance characteristics of this Huygens source antenna are shown in Figs. 8(b) and 8(c). Fig. 8(b) demonstrates that the antenna is well-matched to the source at the resonance frequency f_{res} = 299.39 MHz with $|S_{11}|_{min}$ = −17.04 dB. Thus, ka = 0.45. The antenna remains electrically small and very low profile ($\sim\lambda_{res}/78$). Figs. 8(c) and 9 clearly demonstrate that it radiates as a Huygens source broadside to the plane of the antenna, i.e., along the z-axis.

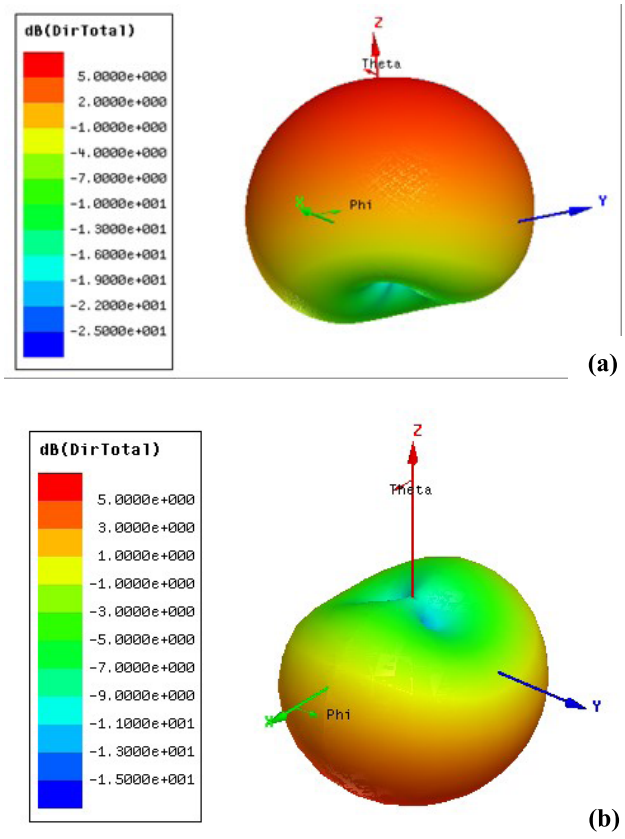

FIGURE 9. HFSS-predicted 3D directivity patterns of the Huygens source antenna with four CLL and one EAD NFRP elements. (a) OZ = 7.55 mm at f_{res} = 299.39 MHz, and (b) OZ = 7.8 mm at f_{res} = 299.54 MHz.

The FTBR = 281.62 (24.50 dB). The accepted power AP = 0.980 W and the total radiated power RP = 0.887 W, giving the radiation efficiency RE = 90.5%. The maximum directivity D_{max} = 3.20 (5.05 dB). The peak realized gain RG_{max} = 2.84 (4.53 dB). The 3dB bandwidth is 0.55 MHz (giving a fractional bandwidth FBW = 0.18%). Contrasting Figs. 9(a) and 9(b), one again finds the phase change when OZ is too large, causing the peak of the directivity to reverse its direction.

This case does demonstrate several interesting facts. First, despite the presence of more copper, the radiation efficiency increases. Second, the FTBR ratio is increased with more power radiated by the combined set of four CLL NFRP elements. Third, even with two more resonators, the bandwidth of the overall system only decreases slightly. This five NFRP element case also confirms several observations made with the previous three element case. The inductance was increased with the presence of the two additional CLL elements, allowing for a small decrease in the capacitance loading each of them to keep the resonance frequency about the same. The length of the driven dipole increased slightly, providing a small amount of inductance to retune the matching in the presence of more capacitive couplings. The distance OZ had to be increased slightly to compensate for the additional magnetic dipole radiators and the associated shift in their overall phase center. Increasing OZ too much does induce the same phase change observed with the smaller number of NFRP elements.

VI. CONCLUSION

Two very low profile, broadside radiating, electrically small Huygens source antennas were demonstrated. The individual metamaterial-inspired electric- and magnetic-based NFRP antennas used to construct these Huygens sources were first designed to have high individual radiation efficiencies and overlapping resonance behaviors. The radiation performance characteristics of these electrically small antennas were presented. The integration of their NFRP elements to realize a Huygens source antenna was explained. With only a few parameter changes, an optimized configuration was demonstrated that achieved high radiation efficiency and FTBR values near 300 MHz. The important physical effects required to secure the Huygens source behavior were elucidated. A 5 NFRP element extension of the 3 element case confirmed and emphasized these properties.

The presence of the lumped elements in the designs allows for frequency tuning of the individual NFRP elements and, hence, the overall antenna. This has been demonstrated previously with each NFRP element separately for both frequency agile and instantaneous bandwidth considerations using lumped elements with different values, embedded varactors, and non-Foster circuits [17], [23], [24], [27]–[29]. Moreover, while the lumped elements were modeled as ideal components in the presented designs, approaches of how to manage the tolerance, parasitic and resistive loss issues associated with real components which will impact, for example, the resonance frequency and overall efficiency have been developed through previous NFRP antenna experiences. It is clear from the current results that small variations in the component values may have unintentional effects on the outcomes and, hence, care in any fabricated design must be exercised. Moving to other frequencies may also simplify some of the component considerations. These issues are being considered for the practical realization of prototypes based on the reported designs.

Continuing investigations are emphasizing further simplifications of the design with yet smaller components and to specific frequencies of technological interest. The ability to have an electrically small antenna that radiates efficiently in the broadside direction with no back radiation opens exciting new avenues to explore directional emission mechanisms and has many immediate applications in a variety of commercial and military wireless systems.

ACKNOWLEDGMENT

Contributions to this work occurred while the author was the 2014-2015 Australian DSTO Fulbright Distinguished Chair in Advanced Science and Technology. He especially would like to thank the Australian-American Fulbright Commission

and the Defense Sciences and Technology Group (formally DSTO) for their support.

REFERENCES

[1] R. F. Harrington, "On the gain and beamwidth of directional antennas," *IEEE Trans. Antennas Propag.*, vol. 6, no. 3, pp. 219–225, Jul. 1958.

[2] R. F. Harrington, "Effect of antenna size on gain, bandwidth, and efficiency," *J. Res. Nat. Bureau Standards*, vol. 64D, no. 1, pp. 1–12, Jan./Feb. 1960.

[3] C. A. Balanis, *Antenna Theory: Analysis and Design*, 3rd ed. Hoboken, NJ, USA: Wiley, 2005.

[4] A. D. Yaghjian, T. H. O'Donnell, E. E. Altshuler, and S. R. Best, "Electrically small supergain end-fire arrays," *Radio Sci.*, vol. 43, no. 3, pp. 1–13, 2008.

[5] S. R. Best, E. E. Altshuler, A. D. Yaghjian, J. M. McGinthy, and T. H. O'Donnell, "An impedance-matched 2-element superdirective array," *IEEE Antennas Wireless Propag. Lett.*, vol. 7, pp. 302–305, 2008.

[6] S. Lim and H. Ling, "Design of electrically small Yagi antenna," *Electron. Lett.*, vol. 43, no. 5, pp. 3–4, Mar. 2007.

[7] S. Lim and H. Ling, "Design of a closely spaced, folded Yagi antenna," *IEEE Antennas Wireless Propag. Lett.*, vol. 5, no. 1, pp. 302–305, Dec. 2006.

[8] F. Yang and Y. Rahmat-Samii, *Electromagnetic Band Gap Structures in Antenna Engineering*. Cambridge, U.K.: Cambridge Univ. Press, 2009.

[9] R. F. J. Broas, D. F. Sievenpiper, and E. Yablonovitch, "A high-impedance ground plane applied to a cellphone handset geometry," *IEEE Trans. Microw. Theory Tech.*, vol. 49, no. 7, pp. 1262–1265, Jul. 2001.

[10] S. Clavijo, R. E. Diaz, and W. E. McKinzie, "Design methodology for Sievenpiper high-impedance surfaces: An artificial magnetic conductor for positive gain electrically small antennas," *IEEE Trans. Antennas Propag.*, vol. 51, no. 10, pp. 2678–2690, Oct. 2003.

[11] R. Coccioli, F.-R. Yang, K.-P. Ma, and T. Itoh, "Aperture-coupled patch antenna on UC-PBG substrate," *IEEE Trans. Microw. Theory Tech.*, vol. 47, no. 11, pp. 2123–2130, Nov. 1999.

[12] A. Erentok, P. L. Luljak, and R. W. Ziolkowski, "Characterization of a volumetric metamaterial realization of an artificial magnetic conductor for antenna applications," *IEEE Trans. Antennas Propag.*, vol. 53, no. 1, pp. 160–172, Jan. 2005.

[13] P. Jin and R. W. Ziolkowski, "Metamaterial-inspired, electrically small Huygens sources," *IEEE Antennas Wireless Propag. Lett.*, vol. 9, pp. 501–505, 2010.

[14] T. Niemi, P. Alitalo, A. O. Karilainen, and S. A. Tretyakov, "Electrically small Huygens source antenna for linear polarisation," *IET Microw. Antennas Propag.*, vol. 6, no. 7, pp. 735–739, 2012.

[15] M.-C. Tang and R. W. Ziolkowski, "Efficient, high directivity, large front-to-back-ratio, electrically small, near-field-resonant-parasitic antenna," *IEEE Access*, vol. 1, pp. 16–28, 2013.

[16] M.-C. Tang, R. W. Ziolkowski, S. Xiao, and M. Li, "A high-directivity, wideband, efficient, electrically small antenna system," *IEEE Trans. Antennas Propag.*, vol. 62, no. 12, pp. 6541–6547, Dec. 2014.

[17] R. W. Ziolkowski, M.-C. Tang, and N. Zhu, "An efficient, broad bandwidth, high directivity, electrically small antenna," *Microw. Opt. Technol. Lett.*, vol. 55, no. 6, pp. 1430–1434, Jun. 2013.

[18] J. P. S. Wong, M. Selvanayagam, and G. V. Eleftheriades, "Design of unit cells and demonstration of methods for synthesizing Huygens metasurfaces," *Photon. Nanostruct. Fundam. Appl.*, vol. 12, no. 4, pp. 360–375, Aug. 2014.

[19] A. Epstein and G. V. Eleftheriades, "Passive lossless Huygens metasurfaces for conversion of arbitrary source field to directive radiation," *IEEE Trans. Antennas Propag.*, vol. 62, no. 11, pp. 5680–5695, Nov. 2014.

[20] C. Pfeiffer and A. Grbic, "Metamaterial Huygens' surfaces: Tailoring wave fronts with reflectionless sheets," *Phys. Rev. Lett.*, vol. 110, no. 19, p. 197401, May 2013.

[21] R. W. Ziolkowski, P. Jin, and C.-C. Lin, "Metamaterial-inspired engineering of antennas," *Proc. IEEE*, vol. 99, no. 10, pp. 1720–1731, Oct. 2011.

[22] ANSYS Corp. *ANSYS HFSS, Ver. 14.0*. [Online]. Available: http://www.ansys.com/Products/Electronics/ANSYS+HFSS, accessed Dec. 10, 2015.

[23] N. Zhu and R. W. Ziolkowski, "Broad-bandwidth, electrically small antenna augmented with an internal non-Foster element," *IEEE Antennas Wireless Propag. Lett.*, vol. 11, pp. 1116–1120, 2012.

[24] N. Zhu and R. W. Ziolkowski, "Broad bandwidth, electrically small, non-Foster element-augmented antenna designs, analyses, and measurements," *IEICE Trans. Commun.*, vols. E96-B, no. 10, pp. 2399–2409, Oct. 2013.

[25] P. Jin and R. W. Ziolkowski, "Multi-frequency, linear and circular polarized, metamaterial-inspired, near-field resonant parasitic antennas," *IEEE Trans. Antennas Propag.*, vol. 59, no. 5, pp. 1446–1459, May 2011.

[26] M. Gustafsson, M. Cismasu, and B. L. G. Jonsson, "Physical bounds and optimal currents on antennas," *IEEE Trans. Antennas Propag.*, vol. 60, no. 6, pp. 2672–2681, Jun. 2012.

[27] M.-C. Tang and R. W. Ziolkowski, "Frequency-agile, efficient, circularly polarized, near-field resonant antenna: Designs and measurements," *IEEE Trans. Antennas Propag.*, vol. 63, no. 11, pp. 5203–5209, Nov. 2015.

[28] J. Church, J.-C. S. Chieh, L. Xu, J. D. Rockway, and D. Arceo, "UHF electrically small box cage loop antenna with an embedded non-Foster load," *IEEE Antennas Wireless Propag. Lett.*, vol. 13, pp. 1329–1332, 2014.

[29] N. Zhu and R. W. Ziolkowski, "Design and measurements of an electrically small, broad bandwidth, non-Foster circuit-augmented protractor antenna," *Appl. Phys. Lett.*, vol. 101, no. 2, p. 024107, Jul. 2012.

RICHARD W. ZIOLKOWSKI (M'87–SM'91–F'94) received the Sc.B. degree in physics, magna cum laude with honors, from Brown University, in 1974, the M.S. and Ph.D. degrees in physics from the University of Illinois at Urbana–Champaign, 1975 and 1980, respectively, and the Doctor Technish Honoris Causa degree from the Technical University of Denmark, in 2012. He was the Australian DSTO Fulbright Distinguished Chair in Advanced Science and Technology from 2014 to 2015. He was the Computational Electronics and Electromagnetics Thrust Area Leader with the Lawrence Livermore National Laboratory, Engineering Research Division, before joining the University of Arizona in 1990. He is currently the Litton Industries John M. Leonis Distinguished Professor with the Department of Electrical and Computer Engineering and a Professor with the College of Optical Sciences, University of Arizona. He is also a Distinguished Professor with the Global Big Data Technologies Centre, University of Technology at Sydney.

His research interests include the application of new mathematical and numerical methods to linear and nonlinear problems dealing with the interaction of electromagnetic and acoustic waves with complex linear and nonlinear media, and metamaterials, metamaterial-inspired structures, and their applications-specific configurations. He is a fellow of the Optical Society of America (OSA). He served as the President of the IEEE Antennas and Propagation Society in 2005. He is also actively involved with the URSI, OSA, and SPIE professional societies.